The Cryosphere Discuss., 6, 3703–3732, 2012
www.the-cryosphere-discuss.net/6/3703/2012/
doi:10.5194/tcd-6-3703-2012

The Cryosphere Discussions

Antarctic ice-mass balance 2002 to 2011: regional re-analysis of GRACE satellite gravimetry measurements with improved estimate of glacial-isostatic adjustment

I. Sasgen[1], H. Konrad[1], E. R. Ivins[2], M. R. van den Broeke[3], J. L. Bamber[4], Z. Martinec[5], and V. Klemann[1,*]

[1]Department of Geodesy and Remote Sensing, GFZ German Research Centre for Geosciences, Telegrafenberg A20, 14473, Potsdam, Germany
[2]Jet Propulsion Laboratory, California Institute of Technology, Pasadena, CA 91109-8099, USA
[3]Institute for Marine and Atmospheric Research, Utrecht University, 3508 TA Utrecht, The Netherlands
[4]School of Geographical Sciences, University of Bristol, University Road, Bristol BS8 1SS, UK
[5]School of Cosmic Physics, Dublin Institute for Advanced Studies, 5 Merrion Square, Dublin 4, Ireland
[*]now at: National Oceanography Centre, 6 Brownlow Street, Liverpool L3 5DA, UK

Received: 31 July 2012 – Accepted: 19 August 2012 – Published: 5 September 2012

Correspondence to: I. Sasgen (sasgen@gfz-potsdam.de)

Published by Copernicus Publications on behalf of the European Geosciences Union.

Abstract

We present regional-scale mass balances for 25 drainage basins of the Antarctic Ice Sheet (AIS) from satellite observations of the Gravity and Climate Experiment (GRACE) for the years 2002–2011. Satellite gravimetry estimates of the AIS mass balance are strongly influenced by mass movement in the Earth interior caused by ice advance and retreat during the last glacial cycle. Here, we develop an improved glacial-isostatic adjustment (GIA) estimate for Antarctica using newly available GPS uplift rates, allowing us to more accurately separate GIA-induced trends in the GRACE gravity fields from those caused by current imbalances of the AIS. Our revised GIA estimate is considerably lower than previous predictions, yielding an (upper) estimate of apparent mass change of $48 \pm 18\,\mathrm{Gt\,yr^{-1}}$. Therefore, our AIS mass balance of $-103 \pm 23\,\mathrm{Gt\,yr^{-1}}$ is considerably less negative than previous GRACE estimates. The Northern Antarctic Peninsula and the Amundsen Sea Sector exhibit the largest mass loss ($-25 \pm 6\,\mathrm{Gt\,yr^{-1}}$ and $-126 \pm 11\,\mathrm{Gt\,yr^{-1}}$, respectively). In contrast, East Antarctica exhibits a slightly positive mass balance ($19 \pm 16\,\mathrm{Gt\,yr^{-1}}$), which is, however, mostly the consequence of compensating mass anomalies in Dronning Maud and Enderby Land (positive) and Wilkes and George V Land (negative) due to interannual accumulation variations. In total, 7 % of the area constitute more than half of the AIS imbalance (53 %), contributing $-151 \pm 9\,\mathrm{Gt\,yr^{-1}}$ to global mean sea-level change. Most of this imbalance is caused by long-term ice-dynamic speed up expected to prevail in the future.

1 Introduction

The current mass balance of the Antarctic Ice Sheet (AIS), and its response to a changing global climate, remains challenging to assess due to the sparsity and shortness of meteorological and glaciological instrumental records. Although satellite measurements have considerably improved our knowledge on the state of the AIS, estimating an accurate mass balance and associated contribution to global sea-level change is

TCD
6, 3703–3732, 2012

difficult due to incomplete spatial coverage of the data sets, and/or the diverse processes influencing the satellite measurements. For example, surface-elevation trends of the AIS acquired with laser or radar altimeters need to be corrected for the spatially and temporally heterogenous firn compaction (e.g. Helsen et al., 2008) to infer mass trends; the input-output method (e.g. Rignot et al., 2008; Joughin et al., 2010; Rignot et al., 2011) relies on sometimes uncertain estimates of the surface velocity and ice thickness close to the grounding line.

While determining mass trends directly from satellite gravimetry data of the Gravity and Climate Experiment (GRACE) has substantial advantages over other measurements the accuracy of AIS mass balances from GRACE has been limited by a poorly constrained GIA. The change in volume and extent of the AIS during the last glacial cycle(s) imposed a varying load on the Earth surface, inducing mass movement and surface deformation. Since the mantle material acts as a highly viscous fluid on these millennial time scales, the GIA of the Earth is delayed with respect to the forcing, where the induced response is governed by the viscosity of the Earth's mantle and the temporal evolution of the ice sheet. Despite the major ice retreat associated with the last glacial cycle has ceased in Antarctica, GIA continues, causing an inflow of mantle material and an upward bending of the lithosphere. The GIA-induced trends in the Earth's gravity field and in the surface deformation are now beginning to be detectable in Antarctica by space-geodetic observing systems, such as GRACE and GPS, respectively.

Several glacial reconstructions have been proposed for predicting GIA using viscoelastic Earth models. These are based on geomorphologic constraints on the past ice height and extent (e.g., Ivins and James, 2005), thermomechanical ice sheet modelling (e.g., Huybrechts, 2002; Ritz et al., 2001), and – considering GIA-induced surface deformation and gravity field changes of the Earth – on indicators of the past relative sea level (e.g., Lambeck and Chappell, 2001; Peltier, 2004), as well as a combination of these approaches (e.g. Bassett et al., 2007; Whitehouse et al., 2012a,b). However, due to the sparsity of constraints on the ice sheet evolution during the last glacial cycle, both

TCD
6, 3703–3732, 2012

in space and time, and the ambiguity introduced by the poorly known mantle viscosity beneath Antarctica, the reconstructions and associated GIA predictions substantially differ in their magnitude and spatial pattern, causing a large uncertainty in the mass balance estimates from GRACE (e.g. Chen et al., 2009).

In this context, GPS uplift rates in Antarctica are an important constraint on the GIA. Records of surface deformation dating back to the later 1990s are available from stations of the International GNSS Service (IGS), located close to research stations along the coast of Antarctica. Starting in the year 2007, additional GPS stations were deployed further inland, where the presumed GIA-induced uplift is much larger and less complex to interpret than along the coastal rim of Antarctica. The GPS data now collected are beginning to be a significant advance over the IGS records (Thomas et al., 2011), as they constrain – although with larger uncertainty due to shorter records – GIA in regions where the signal is expected to be large. But in addition to GPS, also GRACE offers a constraint on GIA in Antarctica. The large amount of ice mass retreated from the Filchner-Ronne ice-shelf area in the course of the last glacial cycle produces a peak signal of GIA-induced trends in the gravity field for most glacial reconstructions (e.g. Huybrechts, 2002; Ivins and James, 2005). At the same time, contemporary ice-mass variations of and on floating ice shelves should be "transparent" in the GRACE data, as all mass variation is isostatically compensated by the ocean water.

The aim of the following investigation is to provide more accurate regional mass balances of the AIS based on an improved correction for GIA. We develop this improved GIA estimate by rigorous analysis of available space-geodetic measurements that directly measure the unique signal standout of the process itself. Although our approach resembles the global inversion of GRACE and GPS data presented by Wu et al. (2010), it includes more accurate and spatially dense data regionally. Furthermore, here we base the inversion on a richer ensemble of GIA forward models. It also differs from the approach followed by Ivins and James (2005) and Whitehouse et al. (2012b), which is based on identifying in a suite of GIA scenarios those consistent with present-day GPS uplift rates without attempting to formally minimize the misfits to both

TCD
6, 3703–3732, 2012

space gravimtery and terrestrial GPS data. In contrast to the approach of Riva et al. (2009), altimetry data is not used in our inversion due to the persisting problematic of relating surface-elevation trends to mass trends. Unless stated otherwise, all GRACE mass balance and acceleration values provided represent error-weighted means for the release of GRACE coefficients CSR RL04 and GFZ RL04 for the time period August 2002 to September 2011.

2 Data and methods

2.1 GRACE filtering and inversion

Here, we use 103 monthly mean solutions of the Earth's gravity field derived from data of the GRACE satellites spanning the time interval August 2002 to September 2011. We adopt the GRACE gravity field solutions of release version 4 (RL04) of the processing centres German Research Centre for Geosciences GFZ, Potsdam, Germany, (GFZ RL04; Flechtner, 2007) and the Centre for Space Research at University of Texas, Austin, USA (CSR RL04; Bettadpur, 2007), which are publicly available as Stokes potential coefficients complete to degree and order 60 and 120, respectively, at http://isdc.gfz-potsdam.de/.

The temporal variations in the gravity field are inverted for mass changes of the AIS using the forward modelling approach detailed in Sasgen et al. (2010). This involves the calculation of the gravity field changes induced by a prescribed mass distribution within 25 drainage basins (Fig. 1), which is based on spatially robust constraints from the input-output method (Rignot et al., 2008). The forward model is then regionally adjusted by the method of least squares to fit the GRACE observations. The GRACE-observed and forward-modelled gravity field changes are shown in Fig. 2. The inversion method, which is similar to the one used by Schrama and Wouters (2011) and Jacob et al. (2012), is weakly dependent on the definition of a priori mass distribution and accurate to < 10% (Sasgen et al., 2012a).

TCD
6, 3703–3732, 2012

To isolate present-day ice-mass change and GIA in the GRACE time series we follow a two step procedure. First, we estimate the temporal linear trends in the GRACE gravity fields (Fig. 2). We then perform a first-order global-scale inversion of the peak trend signals in the GRACE data using forward models consisting of six components; (i) present-day ice-mass changes in Greenland, Alaska, Antarctic Peninsula, and the Amundsen Sea Sector, as well as (ii) GIA over North America and Antarctica. The forward models of (i) are based on ICESat surface-elevation changes (Greenland), airborne laser measurement (Alaska) and surface-ice velocities measured by radar (Antarctic Peninsula and Amundsen Sea Sector). The GIA predictions for the Northern Hemisphere are obtained by subjecting a viscoelastic Earth model to the glacial reconstructions NAWI (Zweck and Huybrechts, 2005). Although the glacial reconstructions NAWI is known to have limitations in the ice distribution over, for example, Eurasia, it has the advantage of being mostly independent of assumptions on the viscosity distribution. Both the total sea-level variation during the last glacial cycle and the GIA signal over North America are constrained at a sufficiently accurate level (Sasgen et al., 2012b) for easily isolating and removing this influence on time-varying geoid and crustal displacements in Antarctica.

2.2 GPS data

The GPS uplift rates used in our study are those presented and provided by Thomas et al. (2011). The rates are obtained from time series of vertical motion, with the time span varying from station to station, the longest being from the year 1995 to 2010. The authors provide two sets of corrections for elastic surface deformation arising from present-day ice-mass changes, which are based on mass balance estimates from the input-output method and ice-mass trends derived from ICESat satellite laser altimetry. Since the GPS stations located along the northern Antarctic Peninsula (OHIG2, ROTB, PALM and SMRT) are dominated by the glacier behaviour after the Larsen Ice Shelf break-up in 2002 (Thomas et al., 2011), we only include GPS rates based on their measurements prior to 2002, when surface deformation is presumably dominated by

TCD
6, 3703–3732, 2012

GIA. We thus include 46 GPS estimates of the vertical surface displacement for 35 mostly near-coastal locations as a new constraint on GIA (see Supplement). The GPS uplift rates are corrected for surface deformation arising from the Northern Hemisphere due to GIA (and present-day ice-mass balances), using the first-order global inversion estimate from GRACE. The correction is nearly uniform for all GPS locations amounting to $0.6 \pm 0.2\,\mathrm{mm\,yr^{-1}}$.

3 Improved estimate of Antarctic glacial-isostatic adjustment

In the following, we will distinguish between a GIA prediction – obtained by applying glacial reconstruction to a viscoelastic Earth model assuming a set of Earth model parameters, and a GIA estimate – obtained by inversion of (space-)geodetic measurements. In this sense, the load histories of Ivins and James (2005), Huybrechts (2002) and Peltier (2004) are glacial reconstructions, and the associated present-day Earth response is a GIA prediction. In contrast, the GIA signals inferred by Riva et al. (2009) (Antarctica; from ICESat and GRACE) and Wu et al. (2010) (global; from GPS and GRACE) are considered GIA estimates. Whitehouse et al. (2012a) performed extensive GIA modelling to derive an Antarctic glacial reconstruction validated, in part, with present-day measurements (Whitehouse et al., 2012b). These results can be considered a GIA formal prediction. It should be emphasized that we do not attempt to evaluate the glacial histories our GIA predictions are based upon. Here, we aim at providing a new "geodetic" Antarctic GIA estimate along with its uncertainties hereinafter called the Antarctic glacial-isostatic adjustment estimate version 1 (AGE1). Due to a much broader sampling of the parameter space compared to Wu et al. (2010), AGE1 is largely independent from assumptions on the viscosity distribution or glacial reconstructions. AGE1 represents an GIA estimate, alternative to the predictions of Ivins and James (2005) or Whitehouse et al. (2012a), for correcting GPS, GRACE and altimetry trends in Antarctica.

TCD
6, 3703–3732, 2012

3.1 Modelling of the GIA in Antarctica

We predict GIA with the viscoelastic Earth model of Martinec (2000), which solves the governing equations of a Maxwell-viscoelastic continuum with the spectral-finite element approach and an explicit time scheme. Rotational deformation is implemented, as well as the sea-level equation allowing for the migration of coastlines (Hagedoorn et al., 2007). Here, the Earth model is run with spatial resolutions of spherical-harmonic degree and order 170 (equivalent to 118 km). As free parameters of the model, we consider the viscosity of the upper and lower mantle, η_{UM} and η_{LM}, respectively, as well as the thickness of the elastic lithosphere h_{L}.

We force our viscoelastic Earth model with three load histories, derived from three published glacial reconstructions of the AIS, LH1 (after Huybrechts, 2002, version digitized from publication), LH2 (after Peltier, 2004, publicly avaliable) and LH3 (after Ivins and James, 2005, personal communication). (For LH2, the maximum ice height of the central loading disc was reduced from 765 m to 444 m, to obtain a smooth transition to neighboring discs.) To obtain regional retreat histories, we subdivide the AIS into five sectors (see Supplement); Antarctic Peninsula (AP), Filchner-Ronne Ice Shelf (FRIS), Ross Ice Shelf (RIS), Amery Ice Shelf (AMIS) and the remaining parts, East Antarctica (EAIS). The criteria for the division are 1) to capture areas with substantial ice retreat in all load histories LH1, LH2 and LH3, and to encompass the main clusters of GPS stations recording the regional GIA signals. That is 6 stations in AP, 14 in FRIS, 13 in RIS, 4 in AMIS, and 9 in EAIS . We then predict the GIA-induced rate of radial displacement, u_r (in centre of figure), and rate of geoid-height change, e_r (in centre of mass), for each per-sector subdivision (r = 1 through 5, corresponding to AP, FRIS, RIS, AMIS and remaining parts, EAIS) of each load history LH1, LH2 and LH3, as well as for four different viscosity distributions VD1 through VD4 (Table 1). The thickness of the elastic lithosphere is held constant at 100 km, except for EAIS (150 km) and AP (80 km), where seismic tomography suggest considerably greater and lesser lithosphere thicknesses, respectively (Danesi and Morelli, 2001; Kobayashi and Zhao, 2004).

TCD
6, 3703–3732, 2012

3.2 GRACE and GPS as a constraint on GIA

We estimate GIA-induced fields of e and u for entire Antarctica from the GRACE and GPS data, respectively, by linear combination of the per-sector predictions of loading history (LH1, LH2 and LH3) and viscosity distribution (VD1 through VD4), accounting for a scalar parameters S_r which are obtained from fitting of either geoid rates to GRACE observations (S_r^{GRACE}), displacement rates to GPS (S_r^{GPS}) or both simultaneously ($S_r^{\mathrm{comb.}}$),

$$e_{\mathrm{Total}}(\boldsymbol{\Omega}) = \sum_r S_r \cdot e_r(\boldsymbol{\Omega}), \quad u_{\mathrm{Total}}(\boldsymbol{\Omega}) = \sum_r S_r \cdot u_r(\boldsymbol{\Omega}), \tag{1}$$

where $\boldsymbol{\Omega}$ stands for the spherical colatitude ϑ and longitude φ, hence, $\boldsymbol{\Omega} = (\vartheta, \varphi)$. The scalar parameter S_r can be interpreted as adjustment factors on the ice heights of the glacial reconstruction due to the approximate linearity of the GIA response with respect to the forcing. It is estimated by minimizing the difference between the predicted and observed fields of e and u in the least-squares sense. For the GRACE-based estimate, a single scaling factor is derived, S^{GRACE}, such that the GIA-induced rate of geoid-height change fits the GRACE trends over a latitude- and longitude-limited adjustment area centred over the Filchner-Ronne ice shelf. For the GPS-based estimate, we allow the proportion of the regional retreat to be changed in LH1, LH2 and LH3, and estimate five scaling parameters simultaneously, one for each per-sector load history, S_r^{GPS}, such that predicted and observed rate of radial displacement is minimized at the location of the GPS stations, $u_{\mathrm{Total}}(\boldsymbol{\Omega}_i)$ and $u_{\mathrm{obs.}}(\boldsymbol{\Omega}_i)$, respectively, i = 1 through 46.

The GIA-estimate satisfying both GRACE and GPS observations according to their respective errors, is obtained by the constrained least-squares approach (e.g. Tarantola, 2005). This approach provides a parameter estimate under the condition that it is close to an a priori value – the deviation being governed by the balance of the uncertainties of the data and the a prior parameter (constraint). Again, five per-sector fields $e_r(\boldsymbol{\Omega})$ and $u_r(\boldsymbol{\Omega})$ are summed up for each of the twelve combinations of load history

TCD
6, 3703–3732, 2012

and viscosity distribution, leading to a GIA estimate for entire Antarctica according to Eq. (1). For the simultaneous estimate, $S_r^{\text{comb.}}$, additionally the scaling factor S^{GRACE} obtained from GRACE is introduced as a constraint to the GPS estimate,

$$\mathbf{S}^{\text{comb.}} = \mathbf{S}^{\text{GRACE}} + \left(F^{\mathrm{T}} C_{\text{GPS}}^{-1} F + C_{\text{GRACE}}\right)^{-1} \cdot F^{\mathrm{T}} C_{\text{GPS}}^{-1} \left(\mathbf{u}_{\text{obs}} - F\,\mathbf{S}^{\text{GRACE}}\right), \quad (2)$$

where the symbols are as follows:

$\mathbf{S}^{\text{comb.}} = (S_1^{\text{comb.}}, ..., S_5^{\text{comb.}})^{\mathrm{T}}$
$\mathbf{S}^{\text{GRACE}} = (S_1^{\text{GRACE}}, ..., S_5^{\text{GRACE}})^{\mathrm{T}}$
$F_{ij} = u_j(\mathbf{\Omega}_i)$ (design matrix)
C_{GRACE} covariance matrix of $\mathbf{S}^{\text{GRACE}}$
C_{GPS} covariance matrix of GPS observations
$\mathbf{u}_{\text{obs.}} = (u_{\text{obs.}}(\mathbf{\Omega}_1), ..., u_{\text{obs.}}(\mathbf{\Omega}_{46}))^{\mathrm{T}}$.

It should be noted that although the forcing from each glacial history for AP, FRIS, RIS, AMIS and EAIS is confined by distinct boundaries, the long-wavelength GIA signal covers entire Antarctica, implying that the fit of each parameter S_r is influenced also by $u_{\text{obs.}}(\mathbf{\Omega}_i)$ and $u_{\text{Total}}(\mathbf{\Omega}_i)$ in other sectors.

Since the combination of GRACE and GPS observations in the scaling parameter $\mathbf{S}^{\text{comb.}}$ is sensitive to the parameter and data uncertainties, special care has to be taken in estimating meaningful (co-)variance matrices C_{GRACE} and C_{GPS}. For the scaling factor inferred from GRACE, we estimate errors due to (i) leakage of present-day signal (with and without considering mass variations outside the Amundsen Sea Sector and the Antarctic Peninsula; 29 %), (ii) sensitivity w.r.t. the choice of the adjustment area (variability introduced by subdividing the adjustment area in four sectors; 9 %), (iii) remaining aliasing periods of oceanic tides underneath the FRIS (with and without estimating K_1 and K_2 periods in temporal decomposition; < 5 %), (iv) difference between two dates sets of GRACE coefficients (GFZ RL04 vs. CSR RL04; 9 %), and (v) formal GRACE coefficient uncertainties (< 2 %), adding up to a total uncertainty of 32 % for S_r.

TCD
6, 3703–3732, 2012

Uncertainties for the GPS trends are taken from (Thomas et al., 2011). The sensitivity of our results to the choice of the GPS and GRACE uncertainties is discussed below.

3.3 Statistical approach to mean GIA estimate

To obtain a robust GIA correction, that is as independent as possible from assumptions on the load history and viscosity distribution, we apply the following statistical approach. We perform the estimation procedure of S_r^{GPS}, and $S_r^{\mathrm{comb.}}$ detailed above while permuting

1. load history (LH1, LH2, LH3) and viscosity distribution (VD1 through VD4) for each sector ($3^5 \times 4^5$ possibilities),
2. elastic corrections for GPS uplift rates (2 possibilities; based on input-output method and ICESat),
3. GRACE release (2 possibilities; CSR RL04 and GFZ RL04),

resulting in an ensemble of 995328 samples, where (1) modifies the design matrix F and the GRACE constraint $\mathbf{S}^{\mathrm{GRACE}}$, (2) the GPS observation vector $\mathbf{u}_{\mathrm{obs.}}$ and (3) again the GRACE constraint. In the combination (Eq. 2), the GRACE constraint S_r^{GRACE} for specific load history and viscosity distribution is applied for each sector r. By this, we also obtain an estimate solely based on GRACE within the statistical approach that is simply a recombination of GRACE-scaled per-sector fields. Thus, it is not affected by the elastic correction (2). Likewise, the estimates from GPS, S_r^{GPS}, are affected only little by the GRACE release permutation – merely due to subtracting a different estimate of the Northern Hemisphere contribution to the observed GPS uplift rates.

Finally, the apparent rate of ice-mass change is calculated for each basin and the entire AIS from the ensemble of S_r^{GPS}, $S_r^{\mathrm{comb.}}$ and S_r^{GRACE}, which are applied to the apparent ice-mass change associated with the unscaled fields for each sector, load history and viscosity distribution. For each of the three types (GRACE, GPS, GRACE &

TCD
6, 3703–3732, 2012

GPS comb.) and each of the 995328 samples, the far-field contribution of the Northern Hemisphere GIA and present-day ice mass change is estimated based on the load history and viscosity distribution adopted for the FRIS sector.

3.4 Apparent ice-mass change of GIA correction

Figure 4 shows the apparent rate of AIS mass change for the ensembles of GIA estimates, which are obtained by the sector-wise permutation of the load history, viscosity distribution, elastic correction, and GRACE release, and subsequent fitting to GPS, GRACE, and both data simultaneously. The GRACE signal over the FRIS area requires a downward adjustment of the initial GIA predictions for most combinations of load histories and viscosity distributions. For other sectors, adjustment factors can not be inferred from GRACE, and the FRIS values are applied. The apparent ice-mass change associated with the GIA estimate constrained by GRACE only is $111 \pm 34\,\mathrm{Gt\,yr^{-1}}$. This GIA estimate, however, exhibits a significant error-weighted mean bias to the GPS uplift rates of approximately $-1\,\mathrm{mm\,yr^{-1}}$ (GIA overestimated w.r.t. GPS observations) shown in Fig. 3.

Using only GPS uplift rates for constraining GIA in each sector reduces this bias nearly to zero ($0.01\,\mathrm{mm\,yr^{-1}}$), resulting in a considerably weaker GIA estimate with an apparent mass gain of only $29 \pm 28\,\mathrm{Gt\,yr^{-1}}$. However, for combinations of GIA predictions with a dominant central EAIS signal (for example LH2), the scaling factor is sometimes inverted in sign by adjusting to negative GPS uplift rates with relatively low uncertainties (e.g. DAV1; -68.58° S, 77.97° E). This inversion of the GIA pattern of EAIS creates an artefact of wide-spread subsidence for EAIS, causing a negative GIA correction of apparent mass change for the total AIS (Fig. 4).

Introducing the GRACE scaling factor as an a priori constraint, which means placing some confidence in the GRACE trends and the initial GIA predictions based on LH1, LH2 and LH3, solves this problem. At the same time, the GIA estimate increases in magnitude resulting in an apparent mass change of $48 \pm 18\,\mathrm{Gt\,yr^{-1}}$ associated with the mean field AGE1 (Fig. 4). The error-weighted mean bias of the observed minus

TCD
6, 3703–3732, 2012

predicted uplift rates at the GPS stations is with approximately $-0.1\,\mathrm{mm\,yr^{-1}}$ low, and nearly centred for all five sectors (Fig. 3). Reducing the errors associated with the GRACE scaling factor by 10 percent points increases the apparent mass change by $9\,\mathrm{Gt\,yr^{-1}}$; augmenting the errors by 10 percent points reduces the apparent mass change by $5\,\mathrm{Gt\,yr^{-1}}$.

Table 2 lists the apparent mass change for each of the 25 drainage basins of the AIS for GIA estimate AGE1 (GPS & GRACE comb.). The spatial pattern of the rate of geoid-height change associated with AGE1 is shown in Fig. 1. The reader is encouraged to apply the GIA correction directly to the GRACE coefficients. We therefore provide the GIA estimate AGE1 (GPS & GRACE comb. and GPS only) as fully normalized spherical-harmonic coefficients (Heiskanen and Moritz, 1967) in the Supplement to this paper.

4 Regional-scale trends and accelerations from GRACE

Table 2 presents rates and accelerations of mass changes for the 25 basins of the AIS from GRACE. The mass balance of the AIS is characterized by strong losses along the Antarctic Peninsula and Amundsen Sea sector ($-123 \pm 13\,\mathrm{Gt\,yr^{-1}}$) and moderate gain of mass for East Antarctica ($19 \pm 16\,\mathrm{Gt\,yr^{-1}}$), adding up to total of $-103 \pm 23\,\mathrm{Gt\,yr^{-1}}$. Major mass loss in West Antarctica occurs in basin 21 (Pine Island Glacier; $-51 \pm 3\,\mathrm{Gt\,yr^{-1}}$) and basin 22 (Thwaites glacier system; $-25 \pm 6\,\mathrm{Gt\,yr^{-1}}$). Mass loss along the Antarctic Peninsula is concentrated in the north, basin 25 ($-25 \pm 4\,\mathrm{Gt\,yr^{-1}}$). Applying the alternative, less strong GIA correction based only on GPS uplift rates, results in an AIS mass balance of $-84 \pm 20\,\mathrm{Gt\,yr^{-1}}$, with a considerable larger ice-mass gain for East Antarctica ($33\,\mathrm{Gt\,yr^{-1}}$). Using the alternative GIA estimate has nearly no effect on the mass loss rates for the Antarctic Peninsula and the Amundsen Sea Sector ($<2\,\mathrm{Gt\,yr^{-1}}$). For both GIA estimates, East Antarctica exhibits a bimodal pattern of mass increase in Dronning Maud and Enderby Land (basins 3 to 8) and mass decrease in Wilkes Land (basins 12 to 15).

TCD
6, 3703–3732, 2012

The situation is more diverse for the acceleration estimates from GRACE presented also in Table 2. Acceleration of mass loss (negative in sign) is observed for the Antarctic Peninsula – here, Palmer Land (basin 24; $-6 \pm 2\,\mathrm{Gtyr}^{-2}$), and to a much lesser extent for northern Antarctic Peninsula (basins 25) – as well as for the Amundsen Sea Sector, in particular, the Pine Island, Thwaites and Getz/Hull/Land glacier systems (basins 21, 22 and 23, respectively; $-18 \pm 8\,\mathrm{Gtyr}^{-2}$). For East Antarctica, mass loss acceleration is observed for Wilkes Land (basin 13 and 14; $-5 \pm 7\,\mathrm{Gtyr}^{-2}$, while deceleration (positive in sign; decrease of mass loss) is observed in Dronning Maude and Enderby Land (basins 5, 6 and 7; $14 \pm 8\,\mathrm{Gtyr}^{-2}$). For the entire AIS, mass loss acceleration arising in the Antarctic Peninsula and Amundsen Sea Sector ($-31 \pm 9\,\mathrm{Gtyr}^{-2}$) is compensated about half by mass loss deceleration in East Antarctica ($13 \pm 13\,\mathrm{Gtyr}^{-2}$), adding up to a total of $-14 \pm 12\,\mathrm{Gtyr}^{-2}$.

5 Discussion

Our mass balance for the AIS of $-103 \pm 23\,\mathrm{Gtyr}^{-1}$ is considerably less negative than the early GRACE estimates of Velicogna (2009) ($-143 \pm 73\,\mathrm{Gtyr}^{-1}$; 2002–2009), who applies a mean GIA correction of $176 \pm 76\,\mathrm{Gtyr}^{-1}$ based on the reconstructions of Ivins and James (2005) and Peltier (2004) and a suite of viscosity distributions, as well as Chen et al. (2009) (2002–2009) estimating a range between $-190 \pm 77\,\mathrm{Gtyr}^{-1}$ and $-250\,\mathrm{Gtyr}^{-1}$ (depending on the GIA correction). We obtain agreement within the errors bars with a more recent GRACE-inferred mass balance of $-122 \pm 50\,\mathrm{Gtyr}^{-1}$ (2003–2010) provided by Rignot et al. (2011), which is supported by their estimates based on the input-output method. However, opposed to Rignot et al. (2011), our GRACE estimate includes the northern Antarctic Peninsula ($-25 \pm 4\,\mathrm{Gtyr}^{-1}$), and is therefore approximately $44\,\mathrm{Gtyr}^{-1}$ less negative. Similar values for the northern Antarctic Peninsula of $-35 \pm 8\,\mathrm{Gtyr}^{-1}$ (January 2003 to April 2009) are obtained by the GRACE analysis of (Ivins et al., 2011). Our estimate supports the previous joint inversion estimate for the total AIS based on GRACE and GPS data of $-87 \pm 43\,\mathrm{Gtyr}^{-1}$ (2002–2008) presented

TCD
6, 3703–3732, 2012

by (Wu et al., 2010). But the separation between East and West Antarctica is substantially different – $-102 \pm 11\,\mathrm{Gt\,yr^{-1}}$ and $19 \pm 16\,\mathrm{Gt\,yr^{-1}}$ (this study) versus $-64 \pm 32\,\mathrm{Gt\,yr^{-1}}$ and $-23 \pm 29\,\mathrm{Gt\,yr^{-1}}$ (Wu et al., 2010), respectively — most likely owing to regional differences between the GIA estimates.

In general, the less negative AIS mass balance is primarily a consequence of our reduced GIA correction of $48 \pm 18\,\mathrm{Gt\,yr^{-1}}$, constrained by GPS uplift rates, and GRACE trends over the FRIS. The GPS and GRACE combined GIA estimate shows a error-weighted mean bias of $-0.10\,\mathrm{mm\,yr^{-1}}$ (weighted root-mean-square (WRMS) error of $1.36\,\mathrm{mm\,yr^{-1}}$), which represents a significant improvement with respect to the bias of $-1.2\,\mathrm{mm\,yr^{-1}}$ associated with the GIA prediction of (Whitehouse et al., 2012a,b). The reduced GIA estimate may be due to weaker loading during the last-glacial cycle and/or faster relaxation of the Earth's mantle during the deglaciation phase, resulting from significantly lower asthenosphere viscosities than assumed here. Using GPS data only to estimate GIA, reduces the mean bias to the GPS uplift rates nearly to zero, with a WRMS error also of $1.35\,\mathrm{mm\,yr^{-1}}$. The apparent mass change associated with this GIA estimate is $29 \pm 14\,\mathrm{Gt\,yr^{-1}}$ (3), which reduces the negative AIS mass balance by $19\,\mathrm{Gt\,yr^{-1}}$ from $-103 \pm 23\,\mathrm{Gt\,yr^{-1}}$ to $-84 \pm 23\,\mathrm{Gt\,yr^{-1}}$. Recognizing that GIA is a small signal compared to present-day ice mass changes in the GRACE trends, this GIA estimate based on GPS uplift rates only is also a plausible. Due to our statistical approach, both GIA estimates are insensitive to assumptions on the viscosity distribution and glacial history.

Figure 5 presents the basin-scale mass balance estimates of the AIS from GRACE (GIA correction AGE1), ordered according to the expected signal-to-noise ratio of present-day ice-mass balance value and the sum of propagated GRACE coefficient errors, filtering and inversion uncertainties, and uncertainties of the GIA correction from Table 2. Additionally, the cumulative sum of the basin-scale mass balances are shown. The most dominant imbalances originate from the northern Antarctic Peninsula (basin 25) and the Amundsen and Bellinghausen Sea Sector (basins 20, 21, 22 and 23). Due to the rather weak influence of GIA in these basins and the strong imprint in the GRACE

TCD
6, 3703–3732, 2012

gravity fields, the sum of imbalances amounting to $-151\,\mathrm{Gt\,yr^{-1}}$ is resolved with an accuracy of $\pm 9\,\mathrm{Gt\,yr^{-1}}$ (6 %). Representing only 7 % of the area of the ice sheet, more than half of the mass imbalances (53 %), positive or negative, occurs in these well resolved basins. Evidence of glacier retreat and acceleration of ice flow in these regions (Scambos et al., 2004; Rignot et al., 2011) suggests that these trends mostly reflect long-term changes of the AIS, which are likely to be sustained in the near future. East Antarctica compensates $19 \pm 16\,\mathrm{Gt\,yr^{-1}}$ of the mass loss. But even if all increase in mass observed with GRACE is attributed to snow accumulation, and not GIA, the total AIS mass balance remains significantly negative ($-55 \pm 18\,\mathrm{Gt\,yr^{-1}}$) – more negative than -30 to $-13\,\mathrm{Gt\,yr^{-1}}$ suggested by radar altimetry (1992–2001 Zwally and Giovinetto, 2011). However, mass trends in East Antarctica are strongly influenced by interannual accumulation variability along the coast, limiting the significance of comparing differing observation periods, as well as of extrapolating the total AIS mass balance into the future.

The acceleration terms inferred for each of the 25 basins are shown in Fig. 6, which are ordered identical to the trend estimates depicted in Fig. 5. Substantive accelerations of mass loss (negative in sign) occur in the basins with strongest negative trends (basins 20, 21, 22 and 23 in the Amundsen Sea Sector, and basin 25 of the northern Antarctic Peninsula) as seen in the figure. This supports the conclusion that there exists a persistent imbalance caused by an altered ice-dynamic behaviour. A preliminary comparison with output from the regional atmospheric climate model (RACMO2/ANT Helsen et al., 2008) suggest, however, that about half of the acceleration of $-22 \pm 9\,\mathrm{Gt\,yr^{-2}}$ may be related accumulation variability within the comparably short observation period. The apparent acceleration in Palmer Land (basin 24; $-6 \pm 2\,\mathrm{Gt\,yr^{-2}}$) is nearly completely explained by accumulation variations within the comparably short observation period. Other pronounced examples for other positive accelerations (increase in mass) induced by accumulation events are found in Dronning Maud Land (basin 5) and Enderby Land (basin 7) and the Southern Antarctic Peninsula (basin 24).

TCD
6, 3703–3732, 2012

6 Conclusions

We have provided a revised GIA estimate for Antarctica, AGE1, based on numerical simulations and newly available GPS uplift rates, as well as GRACE trends beneath the Filchner-Ronne-Ice shelf. The residual misfit of surface deformation associated with AGE1 and measured GPS uplift rates in Antarctica is $-0.1\,\mathrm{mm\,yr^{-1}}$, which represents an improvement with respect to the GIA prediction e.g. of Whitehouse et al. (2012b) ($-1.2\,\mathrm{mm\,yr^{-1}}$ weighted mean bias of W12a model, optimum earth model). The apparent ice-mass change of $48 \pm 18\,\mathrm{Gt\,yr^{-1}}$ associated with AGE1 is considerably lower than previous estimates, in particular, compared to the earlier correction $176 \pm 76\,\mathrm{Gt\,yr^{-1}}$ applied by Velicogna and Wahr (2006) based on a combination of ICE5G (Peltier, 2004) and IJ05 (Ivins and James, 2005). The implication is significantly weaker negative AIS mass balance of $-103 \pm 23\,\mathrm{Gt\,yr^{-1}}$ estimated from GRACE for the time period August 2002 to September 2011. For our GIA estimate constrained by GPS uplift rates only, we obtain an even less negative mass balance of AIS ($-84 \pm 23\,\mathrm{Gt\,yr^{-1}}$).

Our regional GIA and GRACE mass balance estimates clearly show that more than half of current Antarctic sea-level contribution (positive or negative) arises from 7 % of the area of the ice sheet; mass loss along the northern Antarctic Peninsula and the in Amundsen Sea Sector amount to $-151 \pm 9\,\mathrm{Gt\,yr^{-1}}$. East Antarctica, in contrast, has a slightly positive mass balance ($19 \pm 16\,\mathrm{Gt\,yr^{-1}}$), exhibiting a bipolar signature of accelerating mass increase in Dronning Maud Land and Enderby Land (basins 5, 6 and 7; $14 \pm 8\,\mathrm{Gt\,yr^{-2}}$) and accelerating mass loss in Wilkes Land and George V Land (basin 13 and 14; $-5 \pm 7\,\mathrm{Gt\,yr^{-2}}$). The preliminary comparison with output from RACMO2/ANT suggests that the temporal signatures in East Antarctica (and Palmer Land, Antarctic Peninsula) are mainly due to interannual accumulation variability; enhanced precipitation in the years 2005 and 2007 as part of variability in the large scale atmospheric circulation have induced these mass anomalies, not changes in ice-dynamic flow. The strong imbalance and acceleration observed for the northern Antarctic Peninsula and the Amundsen Sea Sector ($-151\,\mathrm{Gt\,yr^{-1}}$ and $-22\,\mathrm{Gt\,yr^{-2}}$, respectively), however,

TCD
6, 3703–3732, 2012

clearly reflect increasingly vigorous ice flow (Scambos et al., 2004; Rignot et al., 2008) and are likely to be a sustained sea-level contribution of AIS.

Supplementary material related to this article is available online at: http://www.the-cryosphere-discuss.net/6/3703/2012/tcd-6-3703-2012-supplement.zip.

Acknowledgements. Ingo Sasgen and Hannes Konrad would like to acknowledge support from the Deutsche Forschungsgemeinschaft (DFG, German Research Foundation) through grant SA 1734/2-2 and Volker Klemann through grant KL 2284/1-3 (both SPP1257); IS performed part of this work at the Jet Propulsion Laboratory, California Institute of Technology. We would like to thank the German Space Operations Center (GSOC) of the German AeRISpace Center (DLR) for providing continuously and nearly 100% of the raw telemetry data of the twin GRACE satellites. This work is a contribution to the "Helmholtz Climate Initiative REKLIM" (Regional Climate Change), a joint research project of the Helmholtz Association of German research centres (HGF). Michiel van den Broeke acknowledges support from Utrecht University and the Netherlands Polar Programme. ERI is supported by NASA's Earth Surface and Interior Focus Area and Cryosphere Program: work performed at the Jet Propulsion Laboratory, California Institute of Technology. JLB was partly supported by the European Commission's 7th Framework Programme through grant number 226375. Ice2sea contribution number ice2sea137. ZM acknowledges support from the Grant Agency of the Czech Republic through Grant No. P210/10/2227.

The service charges for this open access publication have been covered by a Research Centre of the Helmholtz Association.

References

Bassett, S., Milne, G., Bentley, M., and Huybrechts, P.: Modelling Antarctic sea-level observations to test the hypothesis of a dominant Antarctic contribution to meltwater pulse IA, Quaternary Sci. Rev., 26, 2113–2127, 2007. 3706

Bettadpur, S.: CSR Level-2 Processing Standards Document for Level-2 Product Release 04, Univ. Texas, Austin, Rev. 3.1, GRACE 327-742 (CSR-GR-03-03), 2007. 3708
Chen, J. L., Wilson, C. R., Blankenship, D., and Tapley, B. D.: Accelerated Antarctic ice loss from satellite gravity measurements, Nat. Geosci., 2, 859–862, doi:10.1038/ngeo694, 2009. 3707, 3717
Danesi, S. and Morelli, A.: Structure of the upper mantle under the Antarctic Plate from surface wave tomography, Geophys. Res. Lett., 28, 4395–4398, 2001. 3711
Flechtner, F.: GFZ Level-2 Processing Standards Document for Level-2 Product Release 04, GeoForschungsZentrum Potsdam, Rev. 1.0, GRACE 327-743 (GR-GFZ-STD-001), 2007. 3708
Hagedoorn, J. M., Wolf, D., and Martinec, Z.: An estimate of global mean sea-level rise inferred from tide-gauge measurements using glacial-isostatic models consistent with the relative sea-level record, Pure Appl. Geophys., 164, 791–818, doi:10.1007/s00024-007-0186-7, 2007. 3711
Heiskanen, W. A. and Moritz, H.: Physical Geodesy, W. H. Freeman Co., London, 1967. 3716
Helsen, M. M., van den Broeke, M. R., van de Wal, R. S. W., van de Berg, W. J., van Meijgaard, E., Davis, C. H., Li, Y., and Goodwin, I.: Elevation changes in Antarctica mainly determined by accumulation variability, Science, 320, 1626–1629, doi:10.1126/science.1153894, 2008. 3706, 3719
Huybrechts, P.: Sea-level changes at the LGM from ice-dynamic reconstructions of the Greenland and Antarctic ice sheets during the glacial cycles, Quaternary Sci. Rev., 21, 203–231, 2002. 3706, 3707, 3710, 3711
Ivins, E. R. and James, T. S.: Antarctic glacial isostatic adjustment: a new assessment, Antarctic Sci., 17, 541–553, 2005. 3706, 3707, 3710, 3711, 3717, 3720
Ivins, E. R., Watkins, M. M., Yuan, D., Dietrich, R., Casassa, G., and Rülke, A.: On-land ice loss and glacial isostatic adjustment at the Drake Passage: 2003–2009, J. Geophys. Res., 116, B02403, doi:10.1029/2010JB007607, 2011. 3717
Jacob, T., Wahr, J., Pfeffer, W. T., and Swenson, S.: Recent contributions of glaciers and ice caps to sea level rise, Nature, 482, 514–518, doi:10.1038/nature10847, 2012. 3708
Joughin, I., Smith, B. E., Howat, I. M., Scambos, T., and Moon, T.: Greenland flow variability from ice-sheet-wide velocity mapping, J. Glaciol., 56, 415–430, 2010. 3706
Kobayashi, R. and Zhao, D.: Rayleigh-wave group velocity distribution in the Antarctic region, Phys. Earth Planet. Interiors, 141, 167–181, doi:10.1016/j.pepi.2003.11.011, 2004. 3711

TCD
6, 3703–3732, 2012

Lambeck, K. and Chappell, J.: Sea-level change throughout the Last-Glacial Cycle, Science, 292, 679–686, doi:10.1126/science.1059549, 2001. 3706

Martinec, Z.: Spectral-finite element approach to three-dimensional viscoelastic relaxation in a spherical earth, Geophys. J. Int., 142, 117–141, 2000. 3711

Peltier, W. R.: Global glacial isostasy and the surface of the ice-age earth: the ICE5G (VM2) model and GRACE, Annu. Rev. Earth Pl. Sci., 32, 111–149, doi:10.1146/annurev.earth.32.082503.144359, 2004. 3706, 3710, 3711, 3717, 3720

Rignot, E., Bamber, J. L., Van Den Broeke, M. R., Davis, C., Li, Y., Van De Berg, W. J., and Van Meijgaard, E.: Recent Antarctic ice mass loss from radar interferometry and regional climate modelling, Nat. Geosci., 1, 106–110, doi:10.1038/ngeo102, 2008. 3706, 3708, 3721, 3727

Rignot, E., Velicogna, I., van den Broeke, M. R., Monaghan, A., and Lenaerts, J.: Acceleration of the contribution of the Greenland and Antarctic ice sheets to sea level rise, Geophys. Res. Lett., 38, L05503, doi:10.1029/2011GL046583, 2011. 3706, 3717, 3719

Ritz, C., Rommelaere, V., and Dumas, C.: Modeling the evolution of Antarctic ice sheet over the last 420 000 years: implications for altitude changes in the Vostok region, J. Geophys. Res., 106, 31943–31964, 2001. 3706

Riva, R. E., Gunter, B. C., Urban, T. J., Vermeersen, B. L., Lindenbergh, R. C., Helsen, M. M., Bamber, J. L., van de Wal, R. S., van den Broeke, M. R., and Schutz, B. E.: Glacial isostatic adjustment over Antarctica from combined ICESat and GRACE satellite data, Earth Planet. Sci. Lett., 288, 516–523, doi:10.1016/j.epsl.2009.10.013, 2009. 3708, 3710

Sasgen, I., Martinec, Z., and Bamber, J.: Combined GRACE and InSAR estimate of West Antarctic ice-mass loss, J. Geophys. Res., 115, F04010, doi:doi:10.1029/2009JF001525, 2010. 3708

Sasgen, I., Broeke, M. v. d., Bamber, J. L., Rignot, E., Sandberg Sørensen, L., Wouters, B., Martinec, Z., Velicogna, I., and Simonsen, S. B.: Timing and origin of recent regional ice-mass loss in Greenland, Earth Planet. Sci. Lett., 333–334, 293–303, doi:10.1016/j.epsl.2012.03.033, 2012a. 3708

Sasgen, I., Klemann, V., and Martinec, Z.: Toward the inversion of GRACE gravity fields for present-day ice-mass changes and glacial-isostatic adjustment in North America and Greenland, J. Geodyn., 59–60, 49–63, doi:10.1016/j.jog.2012.03.004, 2012b. 3709

Scambos, T. A., Bohlander, J. A., Shuman, C. A., and Skvarca, P.: Glacier acceleration and thinning after ice shelf collapse in the Larsen B embayment, Antarctica, Geophys. Res. Lett., 31, L18402, doi:10.1029/2004GL020670, 2004. 3719, 3721

TCD
6, 3703–3732, 2012

Schrama, E. and Wouters, B.: Revisiting Greenland ice sheet mass loss observed by GRACE, J. Geophys. Res., 116, B02407, doi:10.1029/2009JB006847, 2011. 3708

Tarantola, A.: Inverse Problem Theory and Methods for Model Parameter Estimation, Society for Industrial and Applied Mathematics, Philadelphia, 2005. 3712

Thomas, I. D., King, M. A., Bentley, M. J., Whitehouse, P. L., Penna, N. T., Williams, S. D. P., Riva, R. E. M., Lavallee, D. A., Clarke, P. J., King, E. C., Hindmarsh, R. C. A., and Koivula, H.: Widespread low rates of Antarctic glacial isostatic adjustment revealed by GPS observations, Geophys. Res. Lett., 38, L22302, doi:10.1029/2011GL049277, 2011. 3707, 3709, 3714

Velicogna, I.: Increasing rates of ice mass loss from the Greenland and Antarctic ice sheets revealed by GRACE, Geophys. Res. Lett., 36, L19503, doi:10.1029/2009GL040222, 2009. 3717

Velicogna, I. and Wahr, J.: Measurements of time-variable gravity show mass loss in Antarctica, Science, 311, 1754–1756, doi:10.1126/science.1123785, 2006. 3720

Whitehouse, P. L., Bentley, M. J., and Brocq, A. M. L.: A deglacial model for Antarctica: geological constraints and glaciological modelling as a basis for a new model of Antarctic glacial isostatic adjustment, Quaternary Sci. Rev., 32, 1–24, doi:10.1016/j.quascirev.2011.11.016, 2012a. 3706, 3710, 3718

Whitehouse, P. L., Bentley, M. J., Milne, G. A., King, M. A., and Thomas, I. D.: A new glacial isostatic adjustment model for Antarctica: calibrated and tested using observations of relative sea-level change and present-day uplift rates, Geophys. J. Int., 190, 1464–1482, doi:10.1111/j.1365-246X.2012.05557.x, 2012b. 3706, 3707, 3710, 3718, 3720

Wu, X., Heflin, M. B., Schotman, H., Vermeersen, B. L. A., Dong, D., Gross, R. S., Ivins, E. R., Moore, A. W., and Owen, S. E.: Simultaneous estimation of global present-day water transport and glacial isostatic adjustment, Nat. Geosci., 3, 642–646, 2010. 3707, 3710, 3718

Zwally, H. and Giovinetto, M.: Overview and assessment of Antarctic ice-sheet mass balance estimates: 1992–2009, Surv. Geophys., 32, 351–376, doi:10.1007/s10712-011-9123-5, 2011. 3719, 3727

Zweck, C. and Huybrechts, P.: Modelling the Northern Hemisphere ice sheet during the last glacial cycle and glaciological sensitivity, J. Geophys. Res., 110, D07103, doi:10.1029/2004JD005489, 2005. 3709

TCD

6, 3703–3732, 2012

Table 1. Upper and lower mantle viscosity values (Pa s) for the four applied viscosity distributions.

	VD1	VD2	VD3	VD4
η_{UM}	4×10^{20}	2×10^{20}	6×10^{20}	8×10^{20}
η_{LM}	2×10^{21}	5×10^{21}	2×10^{22}	4×10^{22}

TCD
6, 3703–3732, 2012

Table 2. Rate and acceleration of basins-scale ice-mass change from GRACE and revised GIA estimate AGE1. The GRACE estimates represent error-weighted values of GFZ RL04 and CSR RL04 estimates. Time period is August 2002 to September 2011.

Drainage basin	Area (10^3km^2)	GRACE (GIA corr.) $\dot{m}$	GRACE $\ddot{m}$	GIA (AIS+NH) $\dot{m}$	GIA (AIS only) $\dot{m}$	GRACE (no GIA corr.) $\dot{m}$
24	369	4 ± 4	−6 ± 2	3 ± 2	3 ± 2	8 ± 4
25	104	−25 ± 4	−1 ± 2	1 ± 2	1 ± 3	−24 ± 3
Ant. Peninsula	473	−21 ± 6	−7 ± 2	4 ± 3	3 ± 3	−17 ± 5
1	342	9 ± 2	−3 ± 3	5 ± 1	4 ± 2	14 ± 2
18	414	8 ± 6	0 ± 1	4 ± 2	3 ± 2	12 ± 6
19	391	8 ± 3	−1 ± 1	4 ± 2	4 ± 2	12 ± 1
20	195	−38 ± 3	−7 ± 2	1 ± 1	0 ± 1	−38 ± 3
21	235	−51 ± 3	−8 ± 2	1 ± 1	1 ± 1	−50 ± 3
22	175	−25 ± 6	−3 ± 8	1 ± 2	1 ± 2	−24 ± 6
23	96	−12 ± 3	−3 ± 1	0 ± 1	−1 ± 1	−12 ± 3
West Ant.	1848	−102 ± 11	−24 ± 9	16 ± 4	12 ± 5	−87 ± 10
2	738	−6 ± 3	0 ± 3	3 ± 2	3 ± 2	−3 ± 2
3	1582	4 ± 3	−1 ± 3	5 ± 3	4 ± 3	9 ± 2
4	226	12 ± 2	2 ± 3	1 ± 1	1 ± 1	13 ± 2
5	361	5 ± 5	6 ± 2	1 ± 1	1 ± 1	6 ± 5
6	443	5 ± 6	2 ± 5	1 ± 1	1 ± 1	6 ± 6
7	412	13 ± 3	6 ± 4	1 ± 1	1 ± 1	14 ± 3
8	243	15 ± 3	−1 ± 2	0 ± 2	0 ± 2	15 ± 2
9	963	−1 ± 4	0 ± 3	2 ± 3	1 ± 3	2 ± 3
10	335	−1 ± 3	1 ± 3	−1 ± 2	−1 ± 2	−2 ± 3
11	690	9 ± 7	2 ± 3	2 ± 3	1 ± 3	11 ± 6
12	1170	−8 ± 3	0 ± 2	3 ± 2	2 ± 2	−5 ± 2
13	741	−8 ± 3	−2 ± 3	2 ± 1	1 ± 1	−6 ± 3
14	147	−8 ± 2	−3 ± 6	0 ± 1	0 ± 0	−8 ± 2
15	281	−2 ± 1	−1 ± 1	1 ± 1	1 ± 1	−1 ± 1
16	1138	−5 ± 7	2 ± 1	3 ± 4	1 ± 4	−2 ± 5
17	506	−4 ± 5	−2 ± 1	3 ± 2	2 ± 2	−2 ± 5
East Ant.	9976	19 ± 16	13 ± 13	29 ± 8	17 ± 8	48 ± 14
Total AIS	12297	−103 ± 23	−18 ± 16	48 ± 18	32 ± 18	−55 ± 14

TCD
6, 3703–3732, 2012

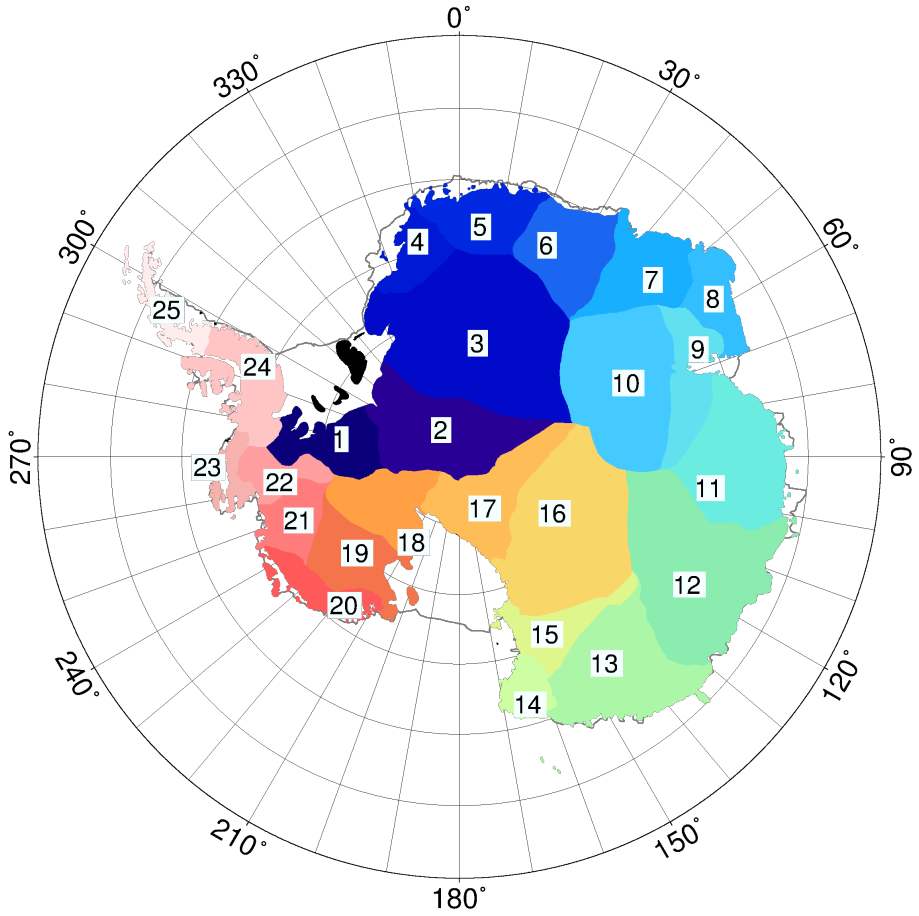

Fig. 1. Division of 25 Antarctic drainage basins investigated in this study (after Rignot et al., 2008; Zwally and Giovinetto, 2011).

TCD
6, 3703–3732, 2012

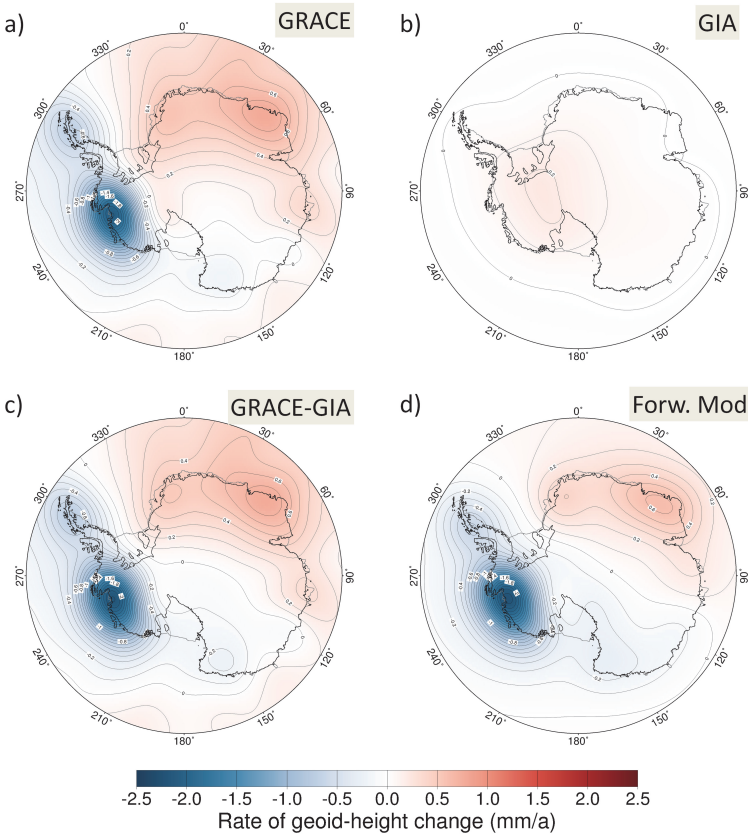

Fig. 2. Rate of geoid-height change ($mm\,yr^{-1}$) from **(a)** GRACE (CSR RL04), **(b)** GIA estimate AGE1 (GRACE & GPS comb.), **(c)** GRACE-GIA estimate AGE1 (present-day ice-mass change), **(d)** forward model adjusted to present-day ice-mass change. Spherical-harmonic cut-off degrees 3 to 60, smoothed with equivalent of ca. 3.6° Gaussian filter.

TCD
6, 3703–3732, 2012

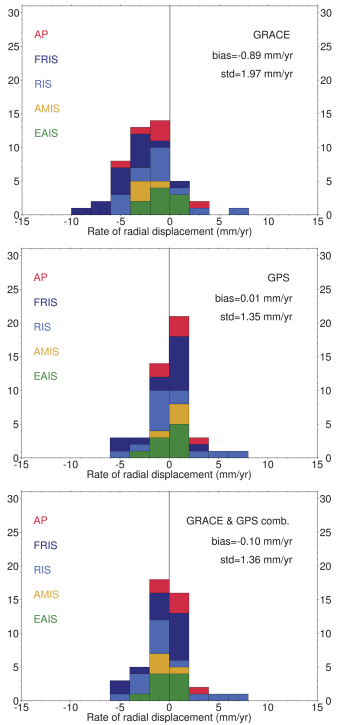

Fig. 3. Observed minus predicted rate of surface deformation at GPS sites. Shown are the residuals in GPS-measured (ICESat elastic and Northern Hemisphere GIA correction applied) minus GIA estimated uplift rates, based on GRACE (top), GPS (middle) and the combination of both observations (bottom). Residuals < 0 (> 0) indicate overestimated (underestimated) GIA with respect to the GPS uplift rates. The residuals are separated for each sector, Antarctic Peninsula (AP; red), Filchner-Ronne Ice Shelf (FRIS; dark blue), Ronne Ice Shelf (RIS; light blue), Amery Ice Shelf (AMIS; yellow) and the remaining parts, East Antarctica (EAIS; green). Also indicated are the weighted mean bias (bias), as well as the weighted root-mean squared error (std).

TCD
6, 3703–3732, 2012

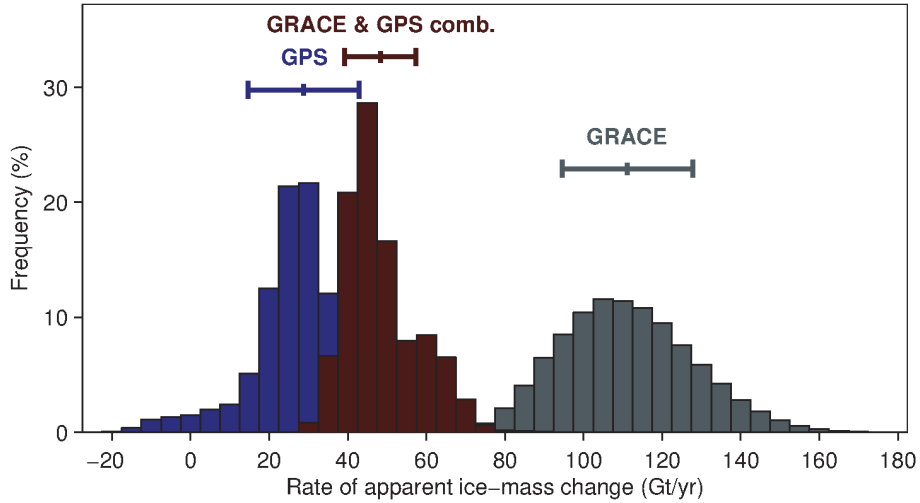

Fig. 4. Distribution of the rate of apparent ice-mass change (Gtyr^{-1}) induced by the GIA, obtained by constraining the ensemble of per-sector combinations (995328 samples) with GPS, GRACE, and both data sets (GRACE & GPS comb.). The apparent ice-mass change is calculated by applying the gravimetric inversion method for the present-day ice-mass changes to each estimate of the GIA-induced gravity field.

TCD
6, 3703–3732, 2012

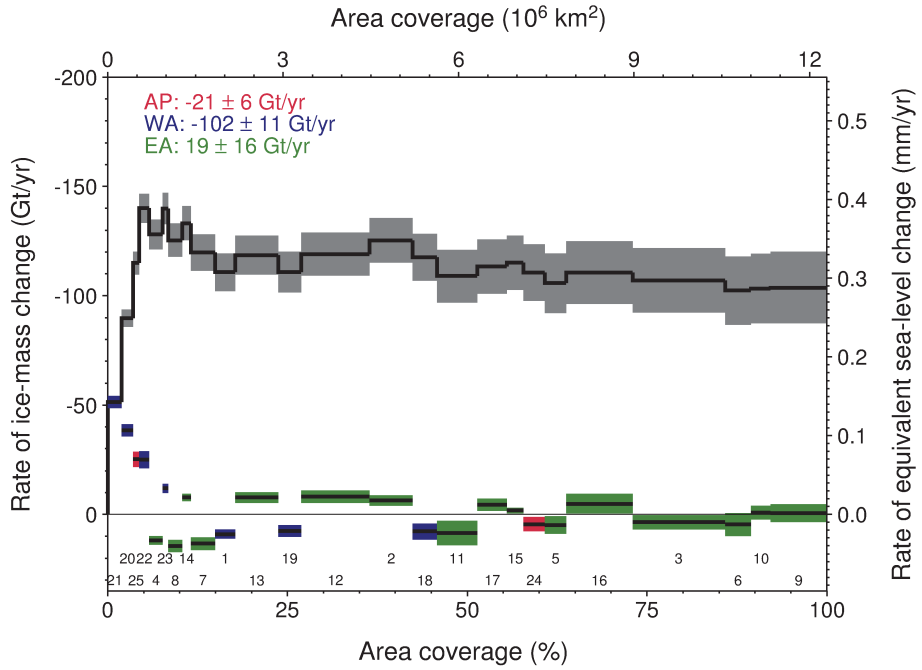

Fig. 5. Rate of basin-scale ice-mass change from GRACE. Shown are the mass balances with uncertainties (bottom part) for each drainage basin of the Antarctic Peninsula (red), West Antarctica (blue) and East Antarctica (green). Numbers in the bottom part of the plot refer to the drainage basin in Fig. 1 and Table 2. The drainage basins are sorted according to the estimated signal to noise ratio. The cumulative sum over the basins is provided in the top part of the figure, depicting that nearly all mass loss originates from a very small portion of the AIS.

TCD
6, 3703–3732, 2012

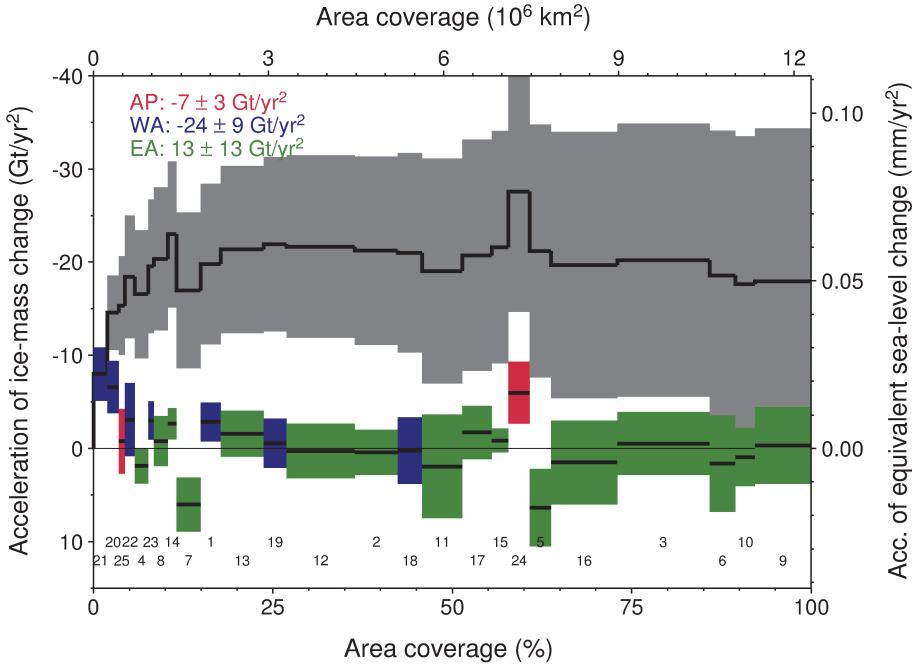

Fig. 6. Same as Fig. 4, but for accelerations of basin-scale ice-mass change from GRACE. The drainage basins are ordered identical to Fig. 4. The much lower accuracy of the acceleration estimate is visible. Also, that strong negative mass balance and strong negative accelerations are correlated for basins of the northern Antarctic Peninsula and Amundsen Sea Sector (20, 21, 22, 23 and 25), supporting evidence for a persistent increase of ice-dynamic flow. For parts of East Antarctica (basins 5, 7 and 13, 4) and Palmer Land (basin 24), comparison with output from the regional atmospheric climate model RACMO2/ANT suggest that the apparent acceleration is caused by interannual accumulation variability.

TCD
6, 3703–3732, 2012